Supplement of Atmos. Chem. Phys., 21, 12631–12647, 2021
https://doi.org/10.5194/acp-21-12631-2021-supplement

Atmospheric Chemistry and Physics
Open Access
EGU

Supplement of

Accelerating methane growth rate from 2010 to 2017: leading contributions from the tropics and East Asia

Yi Yin et al.

Correspondence to: Yi Yin (yiyin@caltech.edu)

Table S1. List of inversions.

Job Name	*Observations*	*OH*	*OH state vector*	*Temporal*
$S1_{Surf\_IN}$	Surface CH_4, CO	INCA	6 big-bands	200904-201712
$S1_{Surf\_TR}$	Surface CH_4, CO	TransCom	6 big-bands	200904-201712
$S2_{GOSATonly\_IN}$	GOSAT CH_4	INCA	Gridded	200904-201712
$S2_{GOSATonly\_TR}$	GOSAT CH_4	TransCom	Gridded	200904-201712
$S3_{Multi\_IN}$	GOSAT CH_4, OMI CH_2O, MOPITT CO	INCA	Gridded	200904-201712
$S3_{Multi\_TR}$	GOSAT CH_4, OMI CH_2O, MOPITT CO	TransCom	Gridded	200904-201712

Table S2. Data sets for the *a priori* CH_4 emissions. A fixed prior is used for all years based 2010 inventories or climatological estimates except for fire emissions that change more irregularly.

Sectors	Annual emissions (Tg yr^{-1})	Data sources
Fossil Fuel Waste	**132**	EDGARv4.2, Olivier and Berdowski (2001) (Janssens-Maenhout et al., 2017)
Coal	*51*	
Oil	*23*	
Gas	*49*	
Energy, industrial, transportation	*8*	
Waste	**62**	
Waste water	*32*	
Solid waste	*30*	
Agriculture	**154**	
Agriculture Soils – Rice	*37.6*	
Agriculture waste burning	*1.6*	
Enteric fermentation	*101.3*	
Manure management	*11.7*	
Wetland	**177**	Kaplan (2002)(Kaplan, 2002) rescaled by P. Bergamaschi (2007) (Bergamaschi et al., 2007)
Fire	**27**	
Biomass Burning (with interannual variations)	*15*	GFED4.1, Van der werf et al., (2017)(van der Werf et al., 2017)
Residential biofuel	*12*	EDGARv4.2
Other		
Termites	**20**	Sanderson, (1996)(Sanderson, 1996)
Ocean	**17**	Lambert and Schmidt (1993)(Lambert and Schmidt, 1993)
Soil deposition	**-38**	Ridgwell et al, (1999)(Ridgwell et al., 1999)
Sum of net surface emissions	**550**	

Table S3. Surface stations included in inversion #S1. Starting or Ending time of the records that do not cover the full study period from 2009.04 – 2017.12 are highlighted in red. The spatial distribution of the stations are shown in Figure S3.

ID	Site Name	Country	Network*	Type	Lat	Lon	Alt	Start time	End Time
ALTcsi	Altert	Canada	CSIRO	flask	82.5	-62.3	210	199104	201712
ALTecc	Altert	Canada	ECCC	flask/in-situ	82.5	-62.3	210	198801	201712
ALTnoa	Altert	Canada	NOAA	flask	82.5	-62.3	201	198506	201712
AMSlsc	Amsterdam Island	France	LSCE	flask/in-situ	-37.8	77.5	70	200310	201507
AMYkma	Anmyeon-do	Korea	KMA	in-situ	36.5	126.3	46	199903	201803
AMYnoa	Anmyeon-do	Korea	NOAA	flask	36.5	126.3	46	201312	201712
ARHniw	Arrival Heights	New Zealand	NIWA	flask	-77.8	166.7	184	198911	201710
ASCnoa	Ascension Island	UK	NOAA	flask	-8.0	-14.4	91	198305	201712
ASKnoa	Assekrem	Algeria	NOAA	flask	23.3	5.6	2710	199509	201712
AZRnoa	Serreta	Portugal	NOAA	flask	38.8	-27.4	40	198305	201712
BHDnoa	Baring Head	New Zealand	NOAA	flask	-41.4	174.9	85	199910	201712
BHDniw	Baring Head	New Zealand	NIWA	flask	-41.4	174.9	85	198908	201712
BKTnoa	Bukit Kototabang	Indonesia	NOAA	flask	-0.2	100.3	864	200401	201712
BMWnoa	Bermuda	UK	NOAA	flask	32.3	-64.9	30	198905	201712
BRWnoa	Barrow	USA	NOAA	flask/in-situ	71.3	-156.6	11	198304	201712
CBAnoa	Cold Bay	USA	NOAA	flask	55.2	-162.7	25	198305	201712
CFAcsi	Cape Ferguson	Australia	CSIRO	flask	-19.3	147.1	2	199106	201712
CGOaga	Cape Grim	Australia	AGAGE	in-situ	-40.7	144.7	94	199308	201709
CGOcsi	Cape Grim	Australia	CSIRO	flask	-40.7	144.7	94	198404	201712
CGOnoa	Cape Grim	Australia	NOAA	flask	-40.7	144.7	94	198404	201712
CHLecc	Churchill	Canada	ECCC	flask/in-situ	58.7	-93.8	16	200704	201712
CHRnoa	Christmas Island	Kiribati	NOAA	flask	1.7	-157.2	3	198403	201712
CMNurb	Monte Cimone	Italy	UNIURB	in-situ	44.2	10.7	2165	200801	201712
CPTnoa	Cape Point	South Africa	NOAA	flask	-34.4	18.5	230	201002	201712
CPTsaw	Cape Point	South Africa	SAWS	in-situ	-34.4	18.5	230	198301	201812

ID	Site Name	Country	Network*	Type	Lat	Lon	Alt	Start time	End Time
CRIcsi	Cape Rama	India	CSIRO	flask	15.1	73.8	60	199302	201301
CRZnoa	Crozet	France	NOAA	flask	-46.4	51.8	120	199103	201712
CYAcsi	Casey	Australia	CSIRO	flask	-66.3	110.6	51	199611	201712
DRPnoa	Drake Passage	USA	NOAA	ship-flask	NA	NA	NA	200304	201712
EGBecc	Egbert	Canada	ECCC	in-situ	44.2	-79.8	255	200503	201712
EICnoa	Easter Island	Chile	NOAA	flask	-27.1	-109.5	50	199401	201706
ESPecc	Estevan Point	Canada	ECCC	in-situ	49.4	-126.5	7	200903	201712
ETLecc	East Trout Lake	Canada	ECCC	in-situ	54.4	-105.0	500	200509	201712
FSDecc	Fraserdale	Canada	ECCC	in-situ	49.8	-81.5	210	199001	201712
GLHuml	Giordan Lighthouse	Malta	UMLT	in-situ	36.1	14.2	167	201201	201712
GMInoa	Guam (Mariana Island)	USA	NOAA	flask	13.4	144.8	2	198305	201706
HBAnoa	Halley	UK	NOAA	flask	-75.6	-25.5	30	198301	201701
HPBnoa	Hohenpeissenberg	Germany	NOAA	flask	47.8	11.0	985	200604	201712
HUNnoa	Hegyhatsal	Hungary	NOAA	flask	47.0	16.7	248	199303	201712
ICEnoa	Storhofdi	Iceland	NOAA	flask	63.4	-20.3	118	199210	201712
IZOnoa	Izaña (Tenerife)	Spain	NOAA	flask	28.3	-16.5	2367	199111	201712
JFJemp	Jungfraujoch	Switzerland	Empa	in-situ	46.5	8.0	3580	200501	201812
KEYnoa	Key Biscane	USA	NOAA	flask	25.7	-80.2	3	198310	201712
KUMnoa	Cape Kumukahi	USA	NOAA	flask	19.5	-154.8	3	198304	201712
LEFnoa	Park Falls	USA	NOAA	flask	45.9	-90.3	868	199411	201712
LAUniw	Lauder	New Zealand	NIWA	flask/in-situ	-45.0	169.7	370	200701	201712
LLBecc	Lac La Biche	Canada	ECCC	in-situ	55.0	-112.5	548	200704	201712
LLBnoa	Lac La Biche	Canada	NOAA	flask	55.0	-112.5	548	200801	201302
LLNnoa	Lulin	Taiwan	NOAA	flask	23.5	120.9	2862	200608	201712
LMPnoa	Lampedusa	Italy	NOAA	flask	35.5	12.6	45	200610	201712
MAAcsi	Mawson	Australia	CSIRO	flask	-67.6	62.9	20	198404	201712

ID	Site Name	Country	Network*	Type	Lat	Lon	Alt	Start time	End Time
MEXnoa	Mex High Alt	Mexico	NOAA	flask	19.0	-97.3	4560	200901	201712
MHDaga	Mace Head	Ireland	AGAGE	in-situ	53.3	-9.9	5	198701	201709
MHDnoa	Mace Head	Ireland	NOAA	flask	53.3	-9.9	5	199106	201712
MIDnoa	Sand Island	USA	NOAA	flask	28.2	-177.4	4	198505	201712
MLOcsi	Mauna Loa	USA	CSIRO	flask	19.5	-155.6	3397	199105	201712
MLOnoa	Mauna Loa	USA	NOAA	flask/in-situ	19.5	-155.6	3397	198309	201712
MNMjma	Minamitorishima	Japan	JMA	in-situ	24.3	154.0	7.1	199401	201802
MQAcsi	Macquarie Island	Australia	CSIRO	flask	-54.5	158.9	6	199004	201712
NATnoa	Natal	Brazil	NOAA	flask	-6.0	-35.2	0	201009	201712
NGLuba	Neuglobsow	Germany	UBAG	in-situ	53.2	13.0	65	199401	201312
NMBnoa	Gobabeb	Namibia	NOAA	flask	-23.6	15.0	408	199701	201712
NWRnoa	Niwot Ridge	USA	NOAA	flask	40.1	-105.6	3523	198305	201712
OXKnoa	Ochsenkopf	Germany	NOAA	flask	50.0	11.8	1185	200303	201712
PALfmi	Pallas	Finland	FMI	in-situ	68.0	24.1	560	200402	201712
PALnoa	Pallas	Finland	NOAA	flask	68.0	24.1	560	200112	201712
PDIvnm	Pha Din	Viet Nam	VNMHA	in-situ	21.6	103.5	1466	201402	201712
POCnoa	Pacific Ocean	USA	NOAA	ship-flask	NA	NA	NA	198612	201707
PRSrse	Plateau Rosa	Italy	RSE	in-situ	45.9	7.7	3480	200501	201712
PSAnoa	Palmer Station	USA	NOAA	flask	-64.8	-64.1	10	198301	201712
PUYlsc	Puy de Dôme	France	LSCE	flask/in-situ	45.8	3.0	1465	200107	201501
RPBaga	Ragged Point	Barbados	AGAGE	in-situ	13.2	-59.4	45	199606	201709
RPBnoa	Ragged Point	Barbados	NOAA	flask	13.2	-59.4	45	198711	201712
RYFjma	Ryofu Maru	Japan	JMA	ship in-situ	NA	NA	NA	199010	201803
RYOjma	Ryori	Japan	JMA	in-situ	39.0	141.8	260	199101	201802
SDZnoa	Shangdianzi	China	NOAA	flask	40.7	117.1	287	200909	201509
SEYnoa	Mahé	Seychelles	NOAA	flask	-4.7	55.2	3	198305	201712

ID	Site Name	Country	Network*	Type	Lat	Lon	Alt	Start time	End Time
SGPnoa	Southern Great Plains	USA	NOAA	flask	36.6	-97.5	318	200204	201712
SHMnoa	Shemya Island	USA	NOAA	flask	52.7	174.1	40	198509	201711
SMOaga	Samoa (Cape Matatula)	USA	AGAGE	in-situ	-14.2	-170.6	77	198507	201709
SMOnoa	Samoa (Cape Matatula)	USA	NOAA	flask	-14.2	-170.6	77	198304	201712
SPOcsi	South Pole	Antarctica	CSIRO	flask	-90.0	-24.8	2841	199103	201712
SPOnoa	South Pole	Antarctica	NOAA	flask	-90.0	-24.8	2841	198302	201712
SSLuba	Schauinsland	Germany	UBAG	in-situ	47.9	7.9	1205	199101	201312
SUMnoa	Summit	Denmark	NOAA	flask	72.6	-38.5	3238	199706	201712
SYOnoa	Syowa	Japan	NOAA	flask	-69.0	39.6	18.4	198691	201712
TAPnoa	Tae-ahn Peninsula	Korea	NOAA	flask	36.7	126.1	20	199011	201712
TERmgo	Teriberka	Russia	MGO	flask	69.2	13.1	40	199001	201712
THDaga	Trinidad Head	USA	AGAGE	in-situ	41.1	-124.2	107	199510	201709
THDnoa	Trinidad Head	USA	NOAA	flask	41.1	-124.2	107	200204	201706
TIKmgo	Tiksi	Russia	MGO	flask	71.6	128.9	8	201009	201712
TIKnoa	Tiksi	Russia	NOAA	flask	71.6	128.9	8	201108	201712
TLLdmc	El Tololo	Chile	DMC	in-situ	-30.2	-70.8	2154	201305	201512
USHnoa	Ushuaia	Argentina	NOAA	in-situ	-54.8	-68.3	18	199409	201712
UTAnoa	Wendover	USA	NOAA	flask	39.9	-113.7	1320	199305	201712
UUMnoa	Ulaan Uul	Mongolia	NOAA	flask	44.5	111.1	914	199201	201712
WISnoa	Sede Boker	Israel	NOAA	flask	31.1	34.9	400	199511	201712
WLGnoa	Mt. Waliguan	China	NOAA	flask	36.3	100.9	3810	199008	201712
WPCnoa	Western Pacific	USA	NOAA	ship-flask	NA	NA	NA	200405	201306
WSAecc	Sable Island	Canada	ECCC	flask/in-situ	43.9	-60.0	2	199911	201712
YONjma	Yonagunijima	Japan	JMA	in-situ	24.5	123.0	30	199801	201802
ZEPnoa	Zeppelin Mountain	Norway	NOAA	flask	78.9	11.9	475	199402	201712
ZSFuba	Zugspitze	Germany	UBAG	in-situ	47.4	11.0	2671	200201	201712

33

*The full names of each network and corresponding site numbers included in this study are listed below.

Network	Site #N	Contributor Name
NOAA	58	Earth System Research Laboratory, National Oceanic and Atmospheric Administration, USA
CSIRO	9	Commonwealth Scientific and Industrial Research Organisation, Australia
ECCC	8	Environment and Climate Change, Canada
AGAGE	5	Advanced Global Atmospheric Gases Experiment Science Team, USA
JMA	4	Japan Meteorological Agency
UBAG	3	Federal Environmental Agency Germany
NIWA	3	National Institute of Water & Atmospheric Research, New Zealand
LSCE	2	Laboratoire des Sciences du Climat et de l'Environnement, France
MGO	2	Voeikov Main Geophysical Observatory, Russia
DMC	1	Direccion Meteorologica de Chile
Empa	1	Swiss Federal Laboratories for Materials Science and Technology
FMI	1	Finnish Meteorological Institute
KMA	1	Korea Meteorological Administration
RSE	1	Ricerca sul Sistema Energetico, Italy
SAWS	1	South African Weather Service
UMLT	1	University of Malta, Malta
UNIURB	1	University of Urbino, Italy
VNMHA	1	Viet Nam Meteorological and Hydrological Administration

Table S4. Summary statistics of monthly growth rates comparison between posterior model states and collocated observations (as shown in Figure 2b and c). Shaded area indicates that the compared observations are assimilated in the corresponding versions.

	Compared to Surface Obs (ppb yr^{-1})		**Compared to GOSAT XCH4 (ppb yr^{-1})**	
	Mean Bias	RMS	Mean bias	RMS
$S1_{Surf}\_IN$	0.44	0.96	0.03	0.45
$S1_{Surf}\_TR$	0.11	0.89	-0.33	0.65
$S2_{GOSATonly}\_IN$	0.05	1.44	-0.2	0.48
$S2_{GOSATonly}\_TR$	0.13	1.55	-0.01	0.68
$S3_{Multi}\_IN$	0.21	1.4	0.07	0.62
$S3_{Multi}\_TR$	0.01	1.48	-0.09	0.7

Figure S1. Regional growth rates of GOSAT X_{CH4} from April 2009 to December 2017. In each subplot, the blue lines represent regional average growth rate in X_{CH4} with orange dashed lines representing the global average as shown in Figure 1b. The regional mask is shown in Figure 5. 18 sub-regions defined in this study include USA, Canada, Central America, Amazon (containing the Northern South America), East Brazil, Southwest South America, Europe, Northern Africa, Tropical Africa, Southern Africa, Russia, Central Asia, Mideast, China, Korea & Japan, South Asia, Southeast Asia, Oceania.

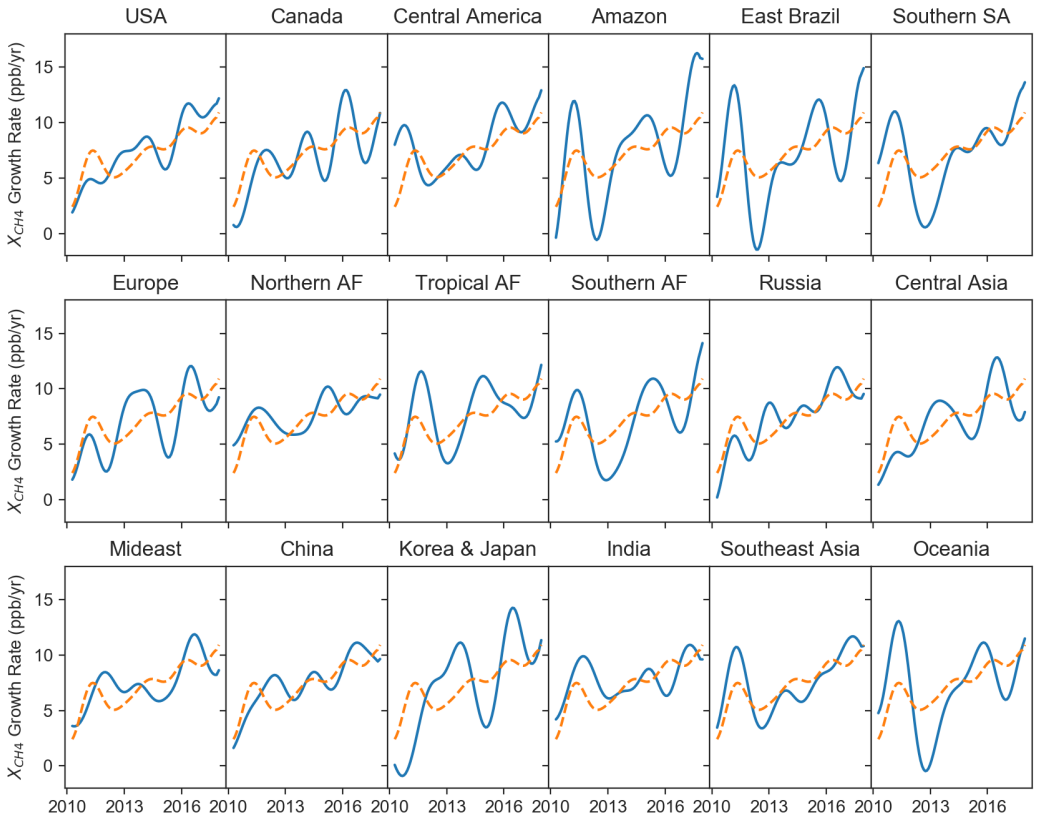

Figure S2. Spatial distribution of surface sites included in inversion #S1. Information on individual stations are listed in Table S3.

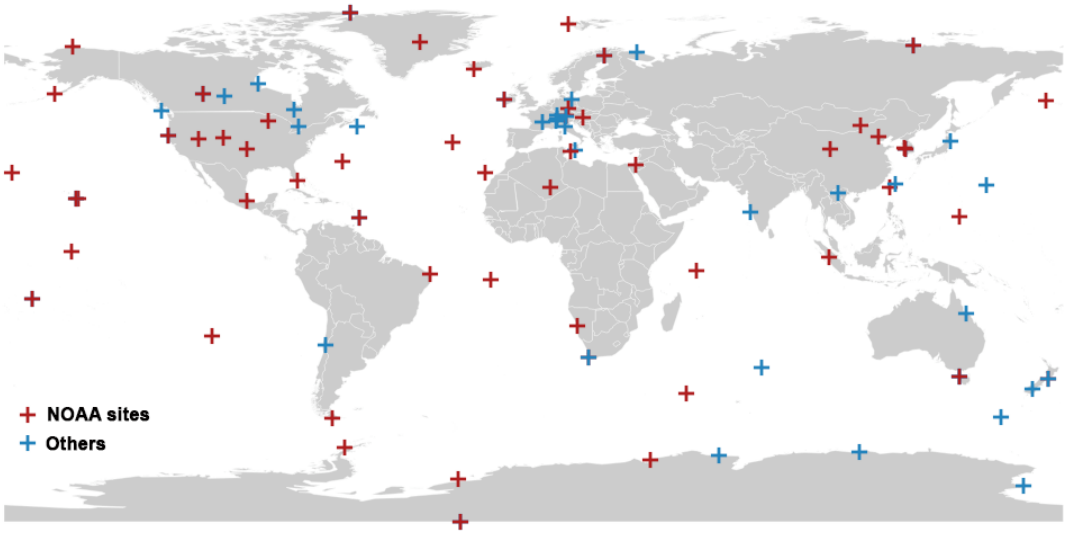

55

Figure S3. Prior emission distributions for the major sectors, namely fossil fuel (oil, gas, coal mining, industry, residential, transport, and geological)**, waste** (landfills and wastewater)**, agriculture** (enteric fermentation, manure management, and rice cultivation), **wetlands** (including inland water), **and fire** (including biofuel). Note that soil deposition (-38 Tg/yr) has been included in the total emissions. Data sources are listed in Table S2.

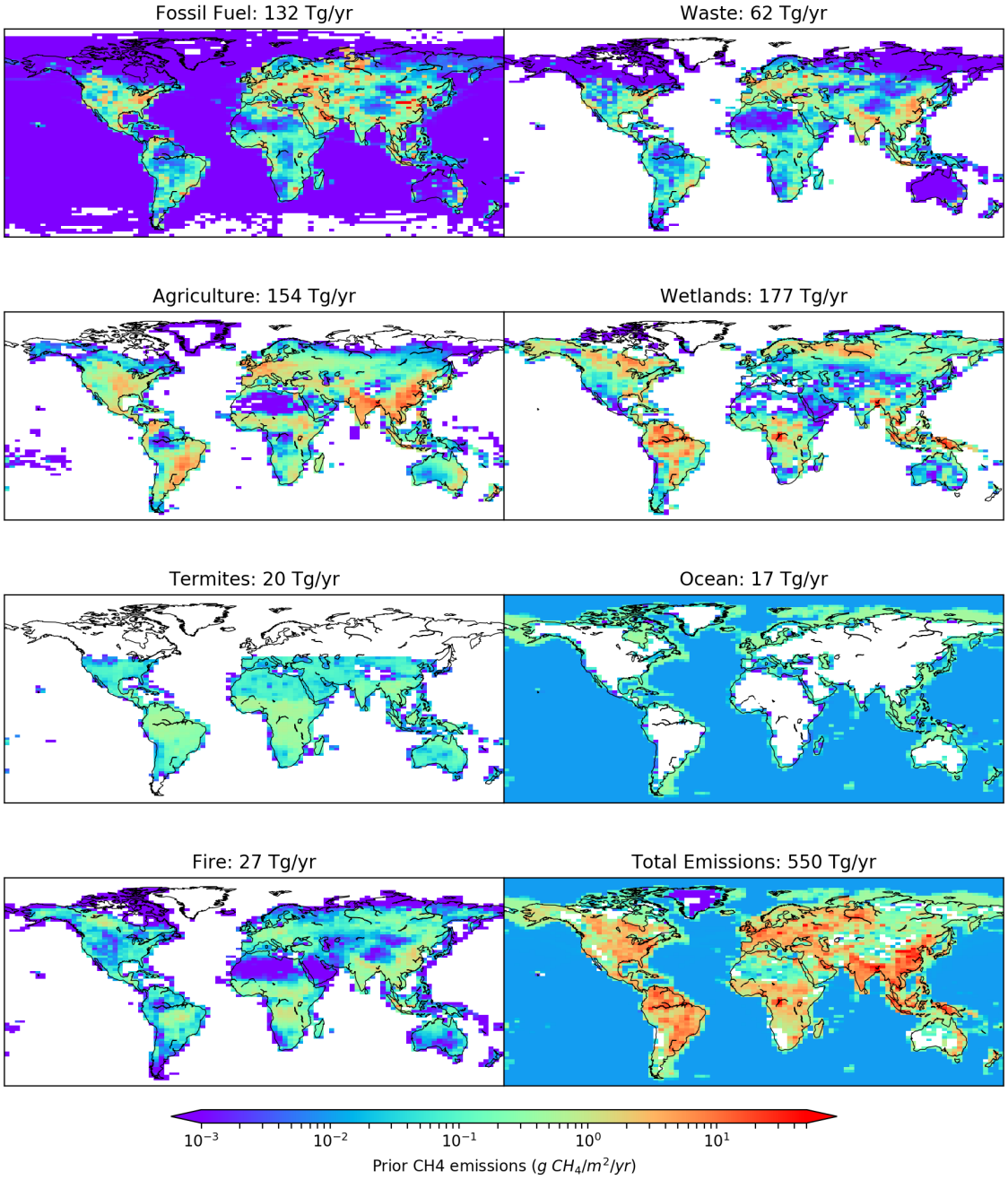

Figure S4. Changes in the zonal OH scaling factors between 2010-2013 and 2014-2017.

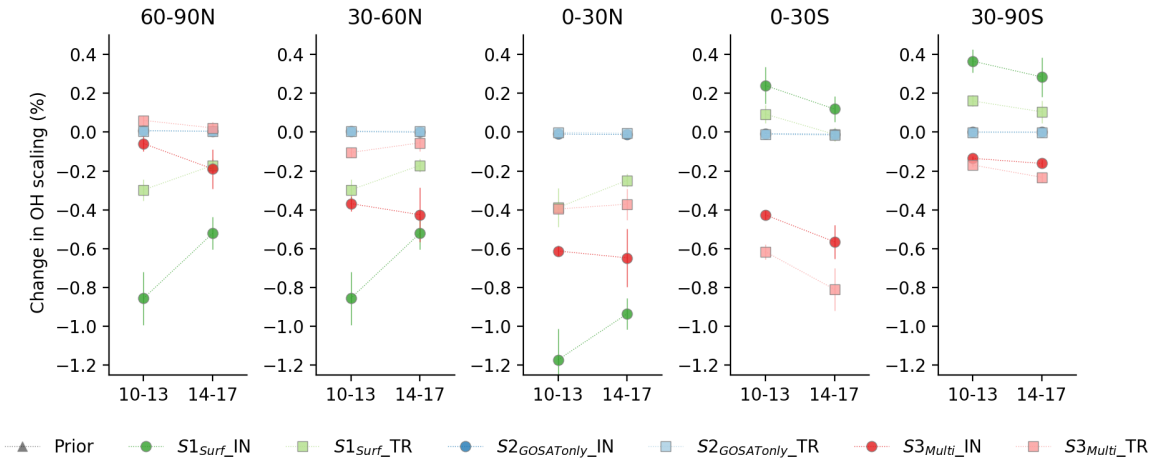

Figure S5. Mean model (a) biases and (b) RMS along the latitude compared to GOSAT X_{CH4} before and after assimilation. Corresponding mean monthly observations numbers are shown in (c). Note individual satellite retrievals are averaged per model grid for every 3 hours for the assimilation (noted as superobs here after). The median observation errors are 20.9 ppb per superobs, and the 5 and 95 percentiles are 19.6 and 24.8 ppb, which includes measurment error (assuming no error correlations between inidividual retrievals) and transport model error (1%). Satellite observations are not assimilated in S1.

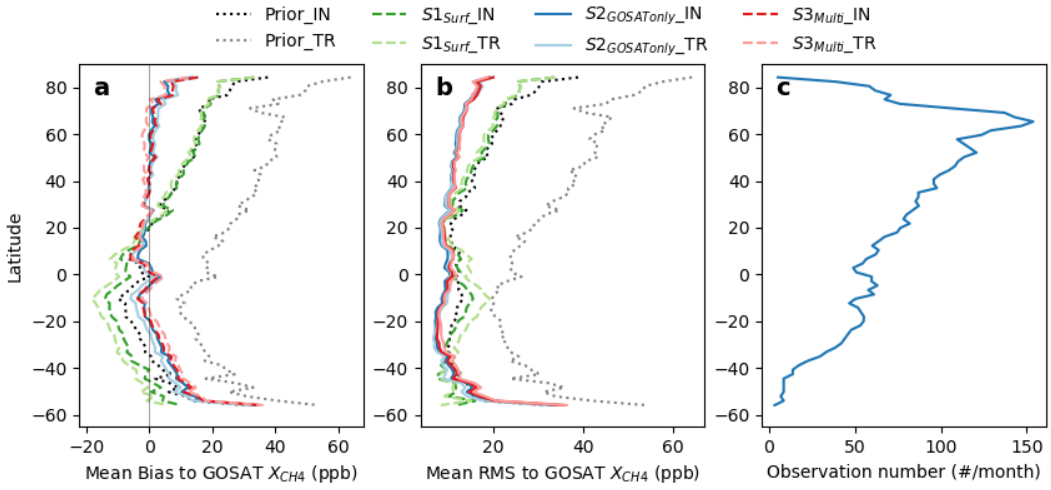

Figure S6. **Monthly mean model (a) biases and (b) RMS compared to GOSAT X_{CH4} before and after assimilation from April 2009 to December 2017.** The global median RMS decreased from 14.5 ppb in the prior modelling with INCA-OH to 8.3 ppb in $S2_{GOSATONLY}$_IN and 8.9 ppb in $S3_{Multi}$_IN, and from 30.7 ppb in the prior modelling with TransCom-OH to 8.5 ppb in $S2_{GOSATONLY}$_TR and 9.1 ppb in $S3_{Multi}$_TR. Note that in S1 (green), satellite observations are not assimilated.

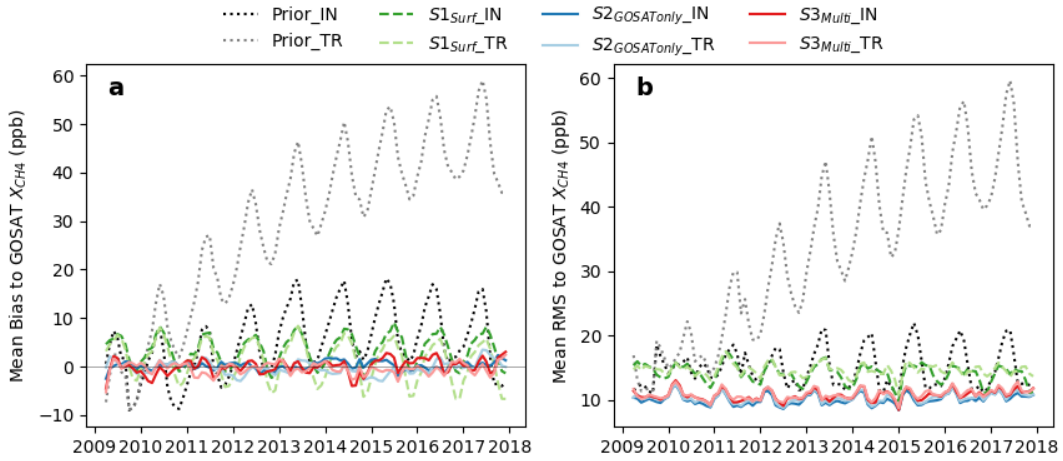

Figure S7. Mean model bias relative to TCCON and surface measurements along the latitude.

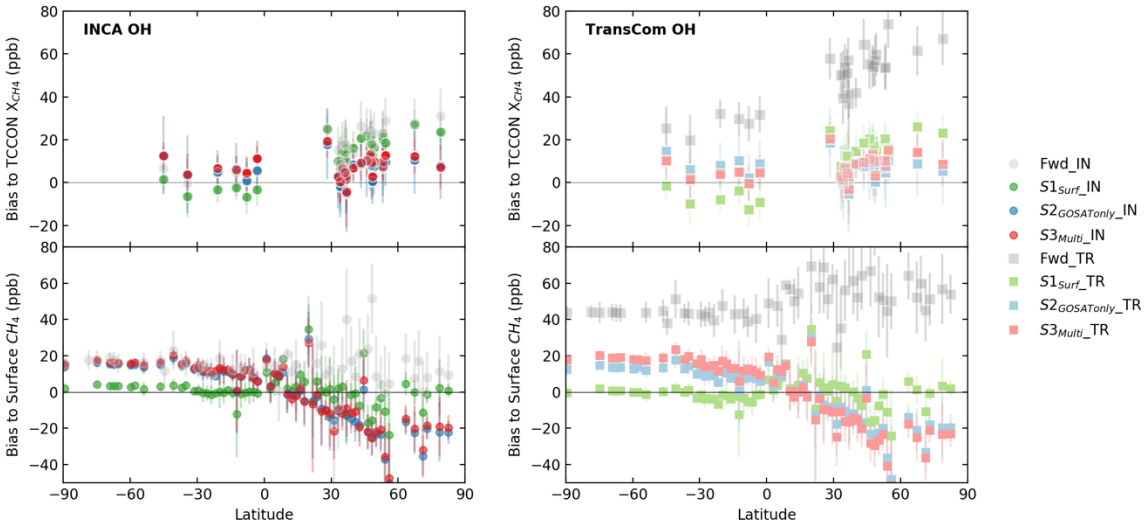

90

Figure S8. Posterior error covariance matrix from the analytical inversion. Results for 2010 is shown here.

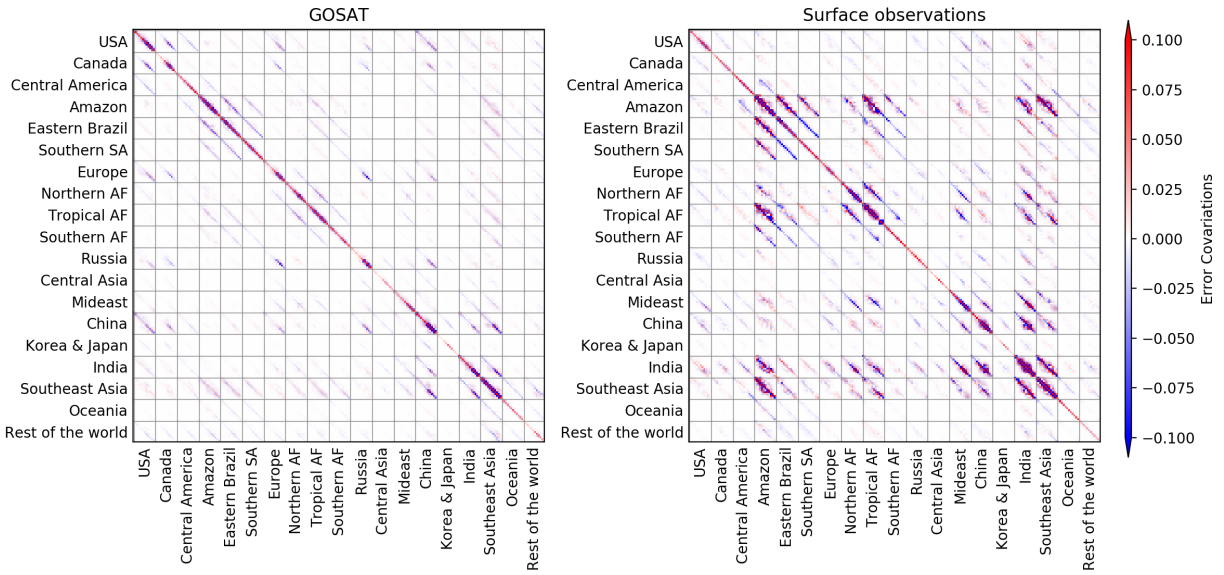

95

Figure S9. Spatial distribution of the relative contributions (%) of the five major sectors in the bottom-up emission estimates used as the prior in this study, namely (a) Fossil Fuel, (b) Waste, (c) Agriculture, (d) Wetland, and (e) Fire. Subplot **(f)** shows the distribution of the dominant sector when its single contribution is larger than 80% of the total CH_4 emissions.

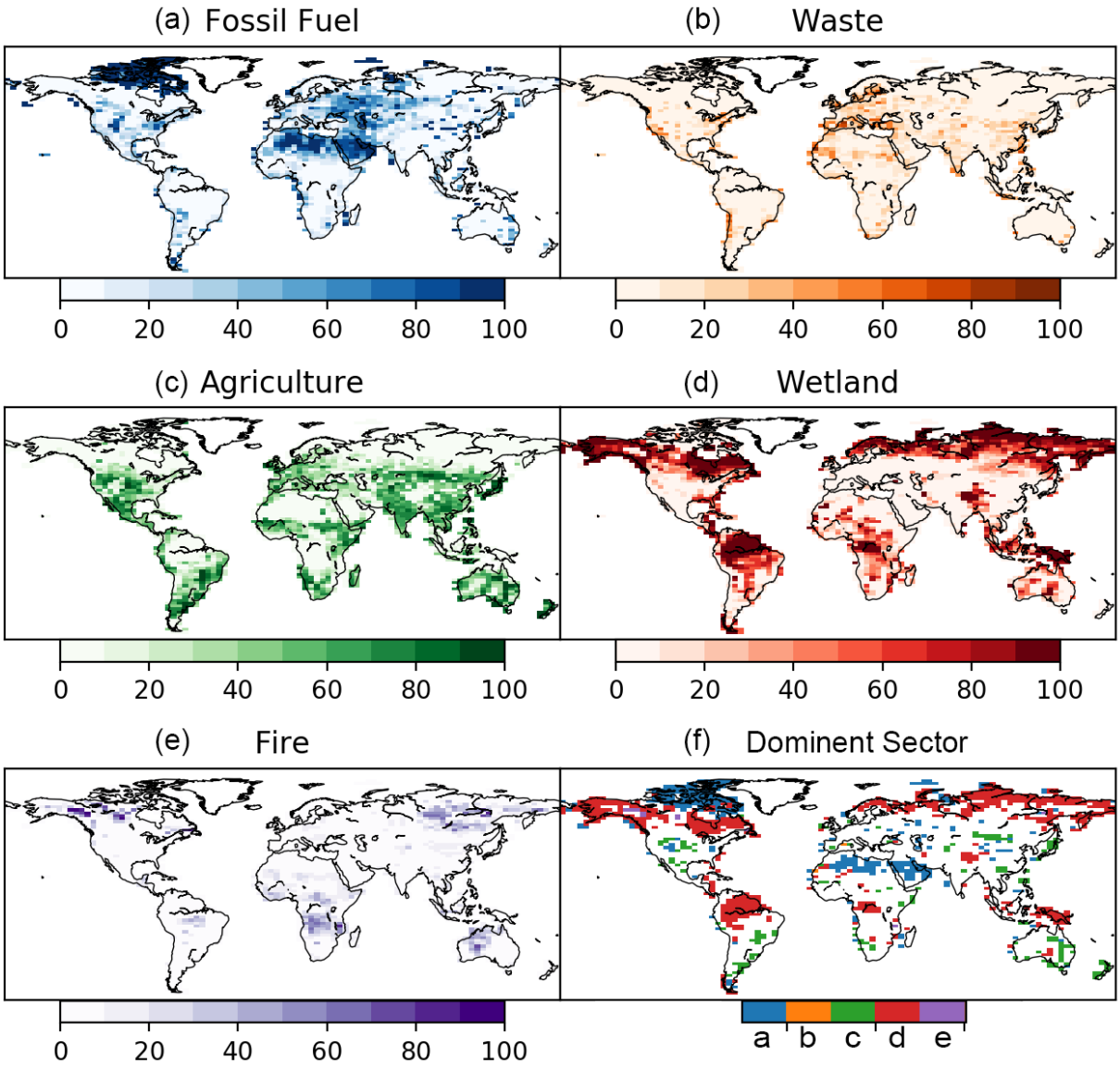

Figure S10. Spatial distribution of the relative contributions (%) of the five major sectors from the most up-to-date bottom-up emission estimates, namely (a) Fossil Fuel, (b) Waste, (c) Agriculture, (d) Wetland, and (e) Fire using a different inventory compared to our prior as shown in Figure S9. Subplot **(f)** shows the distribution of the dominant sector when its single contribution is larger than 80% of the total CH_4 emissions. The anthropogenic sources (fossil fuel, waste, and agriculture) are based the new EDGAR4.3.2 inventories(Janssens-Maenhout et al., 2017), the wetland emissions are based on the ensemble mean of multiple wetland model estimates(Poulter et al., 2017), and fire emissions (including biofuel) are the same as shown in S11a.

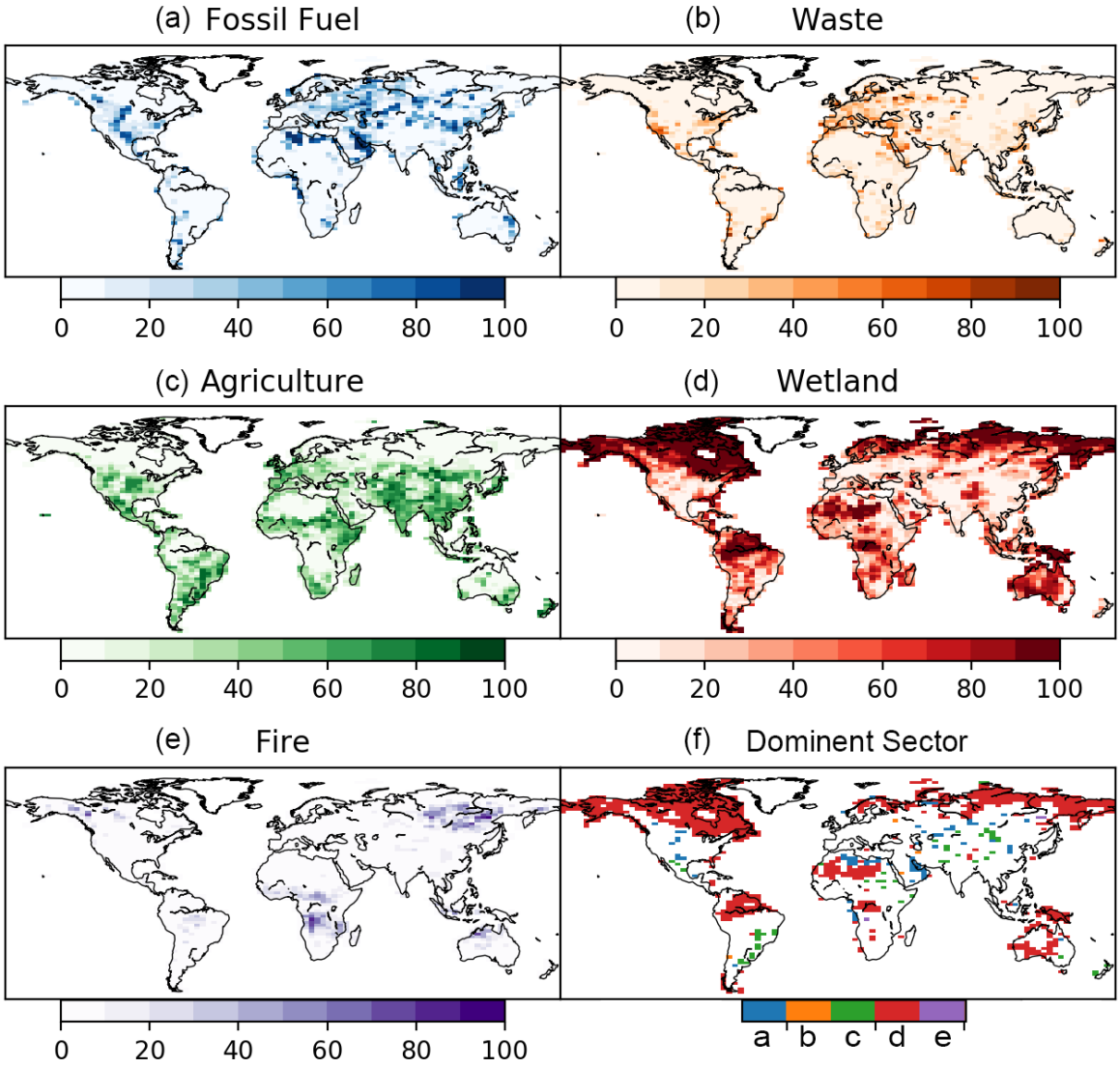

Figure S11. Regional CH_4 emission estimates from inversions and bottom-up inventories. The solid lines represent the six inversion results of this study, where sectoral attribution of the posterior fluxes depend on prior information as shown in Fig. S3. Updated bottom-up inventories are shown here for comparison. The dashed lines show regional anthropogenic emissions based on EDGAR4.3.2 (1970-2012) that are then extrapolated to 2017 using FAO statistics (Saunois et al., 2020), modelled wetland CH_4 emissions from Poulter et al., 2017, and fire emissions from GFED4s and biofuel. The stars denote CEDS (Community Emissions Data System) historical anthropogenic emission estimates updated till 2014 (Hoesly et al., 2018).

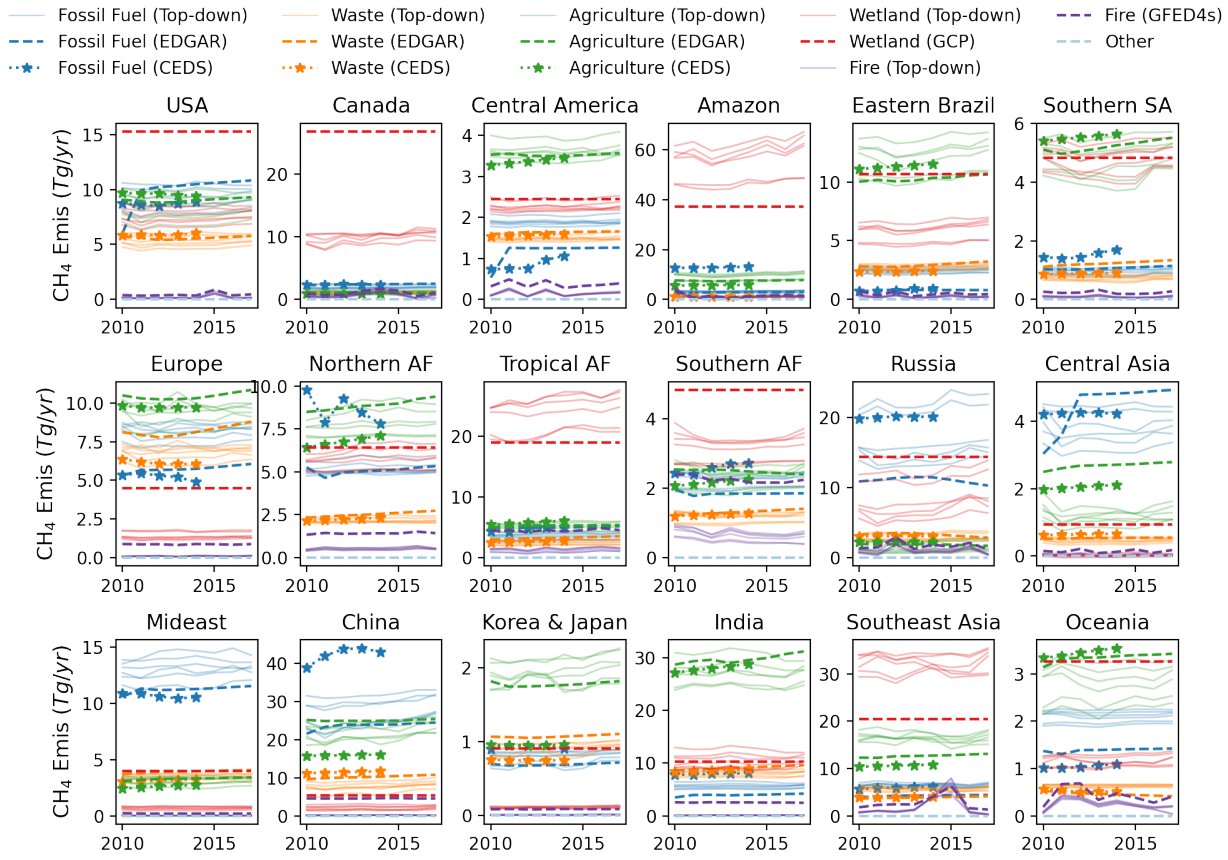

Figure S12. Emission anomalies by sector from the inversion (a) and observed atmospheric $\delta^{13}CH_4$ changes in different latitude zones (b). (a) Emission anomalies relative to the 2010-2013 means are estimated for each version. The mean values are shown in solid lines and the shadings represent 1-sigma standard deviation of estimates from different versions. **(b)** atmospheric $\delta^{13}CH_4$ observed from 19 NOAA background sites. 12-month moving averages are shown here. The dashed lines in late 2017 suggest missing data for the smoothing.

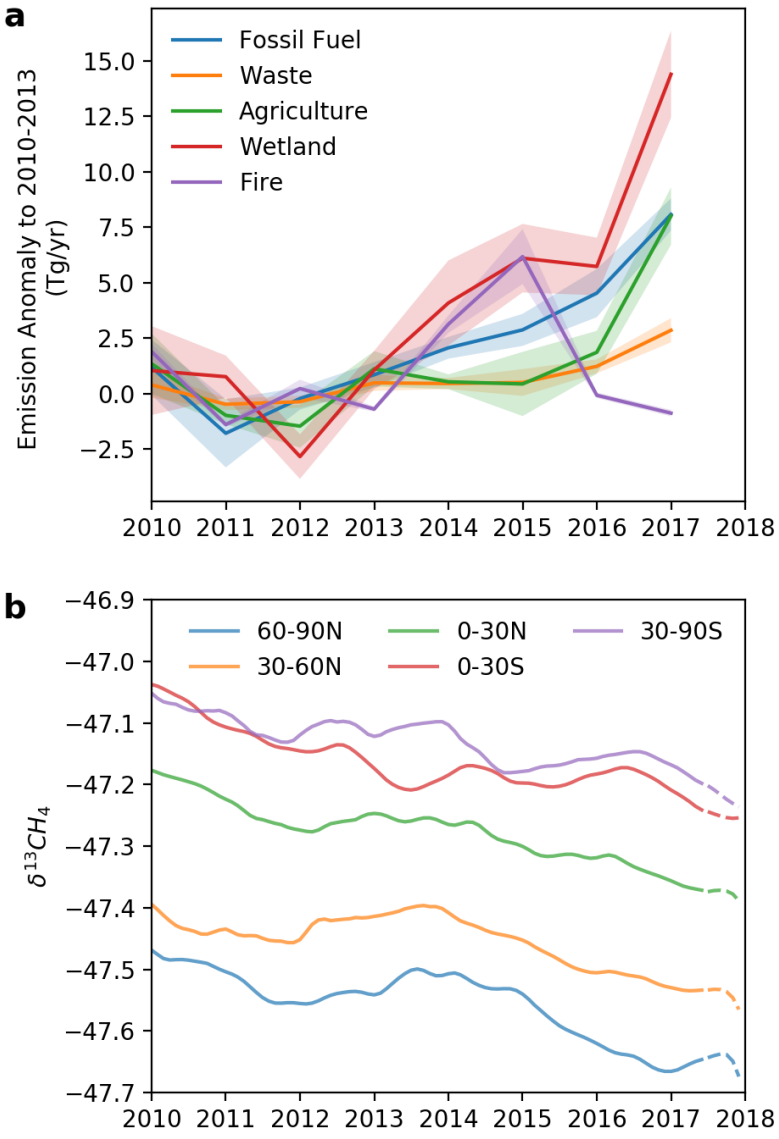

References

Bergamaschi, P., Frankenberg, C., Meirink, J. F., Krol, M., Dentener, F., Wagner, T., Platt, U., Kaplan, J. O., Körner, S., Heimann, M., Dlugokencky, E. J. and Goede, A.: Satellite chartography of atmospheric methane from SCIAMACHY on board ENVISAT: 2. Evaluation based on inverse model simulations, J. Geophys. Res., 112(D2), D02304, doi:10.1029/2006JD007268, 2007.

Hoesly, R. M., Smith, S. J., Feng, L., Klimont, Z., Janssens-Maenhout, G., Pitkanen, T., Seibert, J. J., Vu, L., Andres, R. J., Bolt, R. M., Bond, T. C., Dawidowski, L., Kholod, N., Kurokawa, J., Li, M., Liu, L., Lu, Z., Moura, M. C. P., O'Rourke, P. R. and Zhang, Q.: Historical (1750–2014) anthropogenic emissions of reactive gases and aerosols from the Community Emissions Data System (CEDS), Geosci. Model Dev., 11(1), 369–408, doi:10.5194/gmd-11-369-2018, 2018.

Janssens-Maenhout, G., Crippa, M., Guizzardi, D., Muntean, M., Schaaf, E., Dentener, F., Bergamaschi, P., Pagliari, V., Olivier, J. G. J., Peters, J. A. H. W., van Aardenne, J. A., Monni, S., Doering, U. and Petrescu, A. M. R.: EDGAR v4.3.2 Global Atlas of the three major Greenhouse Gas Emissions for the period 1970–2012, Earth Syst. Sci. Data Discuss., 1–55, doi:10.5194/essd-2017-79, 2017.

Kaplan, J. O.: Modeling the dynamics of terrestrial carbon storage since the Last Glacial Maximum, Geophys. Res. Lett., 29(22) [online] Available from: http://doi.wiley.com/10.1029/2002GL015230, 2002.

Lambert, G. and Schmidt, S.: Reevaluation of the oceanic flux of methane: Uncertainties and long term variations, Chemosphere, 26(1–4), 579–589, doi:10.1016/0045-6535(93)90443-9, 1993.

Poulter, B., Bousquet, P., Canadell, J. G., Ciais, P., Peregon, A., Saunois, M., Arora, V. K., Beerling, D. J., Brovkin, V., Jones, C. D., Joos, F., Gedney, N., Ito, A., Kleinen, T., Koven, C. D., McDonald, K., Melton, J. R., Peng, C., Peng, S., Prigent, C., Schroeder, R., Riley, W. J., Saito, M., Spahni, R., Tian, H., Taylor, L., Viovy, N., Wilton, D., Wiltshire, A., Xu, X., Zhang, B., Zhang, Z. and Zhu, Q.: Global wetland contribution to 2000–2012 atmospheric methane growth rate dynamics, Environ. Res. Lett., 12(9), 094013, doi:10.1088/1748-9326/aa8391, 2017.

Ridgwell, A. J., Marshall, S. J. and Gregson, K.: Consumption of atmospheric methane by soils: A process-based model, Global Biogeochem. Cycles, 13(1), 59–70, doi:10.1029/1998GB900004, 1999.

Sanderson, M. G.: Biomass of termites and their emissions of methane and carbon dioxide: A global database, Global Biogeochem. Cycles, 10(4), 543–557, doi:10.1029/96GB01893, 1996.

Saunois, M., Bousquet, P., Poulter, B., Peregon, A., Ciais, P., Canadell, J. G., Dlugokencky, E. J., Etiope, G., Bastviken, D., Houweling, S., Janssens-Maenhout, G., Tubiello, F. N., Castaldi, S., Jackson, R. B., Alexe, M., Arora, V. K., Beerling, D. J., Bergamaschi, P., Blake, D. R., Brailsford, G., Brovkin, V., Bruhwiler, L., Crevoisier, C., Crill, P., Covey, K., Curry, C., Frankenberg, C., Gedney, N., Höglund-Isaksson, L., Ishizawa, M., Ito, A., Joos, F., Kim, H.-S., Kleinen, T., Krummel, P., Lamarque, J.-F., Langenfelds, R., Locatelli, R., Machida, T., Maksyutov, S., McDonald, K. C., Marshall, J., Melton, J. R.,

Morino, I., Naik, V., O'Doherty, S., Parmentier, F.-J. W., Patra, P. K., Peng, C., Peng, S., Peters, G. P., Pison, I., Prigent, C., Prinn, R., Ramonet, M., Riley, W. J., Saito, M., Santini, M., Schroeder, R., Simpson, I. J., Spahni, R., Steele, P., Takizawa, A., Thornton, B. F., Tian, H., Tohjima, Y., Viovy, N., Voulgarakis, A., van Weele, M., van der Werf, G. R., Weiss, R., Wiedinmyer, C., Wilton, D. J., Wiltshire, A., Worthy, D., Wunch, D., Xu, X., Yoshida, Y., Zhang, B., Zhang, Z. and Zhu, Q.: The global methane budget 2000–2012, Earth Syst. Sci. Data, 8(2), 697–751, doi:10.5194/essd-8-697-2016, 2016.

van der Werf, G. R., Randerson, J. T., Giglio, L., Van Leeuwen, T. T., Chen, Y., Rogers, B. M., Mu, M., Van Marle, M. J. E., Morton, D. C., Collatz, G. J., Yokelson, R. J. and Kasibhatla, P. S.: Global fire emissions estimates during 1997-2016, Earth Syst. Sci. Data, 9(2), 697–720, doi:10.5194/essd-9-697-2017, 2017.